


**Quantum work statistics in regular and classical-chaotic dynamical billiard systems**Sebastian Rosmej and Mattes Heerwagen *Carl von Ossietzky Universität Oldenburg, Institut für Physik, D-26111 Oldenburg, Germany*

(Received 30 November 2021; accepted 5 May 2022; published 26 May 2022)

In the thermodynamics of nanoscopic systems the relation between classical and quantum mechanical description is of particular importance. To scrutinize this correspondence we have chosen two two-dimensional billiard systems. Both systems are studied in the classical and the quantum mechanical settings. The classical conditional probability density  $p(E, L|E_0, L_0)$  as well as the quantum mechanical transition probability  $P(n, l|n_0, l_0)$  are calculated, which build the basis for the statistical analysis. We calculate the work distribution for one particle. The results in the quantum case in particular are of special interest since a suitable definition of mechanical work in small quantum systems is already controversial. Furthermore, we analyze the probability of both zero work and zero angular momentum difference. Using connections to an exactly solvable system analytical formulas are given for both systems. In the quantum case we get numerical results with some interesting relations to the classical case.

DOI: [10.1103/PhysRevE.105.054147](https://doi.org/10.1103/PhysRevE.105.054147)**I. INTRODUCTION**

One crucial ingredient for the thermodynamic characterization of small systems with typical energy turnover of the order of the thermal energy per degree of freedom is the statistical distribution of work [1,2]. In the classical setting the definition of work is unambiguous; it is defined as the integral of force along the trajectory. In the quantum case the definition of work meets some difficulties [3–6].

There exists no analog of the classical trajectory. A possible and intuitive way to define quantum work is to measure the energy twice, before and after the process. This definition is called the two projective measurement method [3,4]. On the one hand, this definition is simple and operative. On the other hand, the measurements are likely to destroy quantum interferences that may be decisive for the nonclassical behavior of the system. To clarify which correlations are destroyed by the two projective measurement prescription and which are kept, it is instructive to look in detail at the correspondence between classical and quantum work distributions [7,8]. This has been done for a quartic oscillator with time-dependent stiffness constant [9,10] and for a periodically driven quartic oscillator [11]. The latter system shows chaotic behavior in some regions of parameter space. In this paper we extend the analysis to billiards with moving walls that are known to implement fully chaotic motion.

Billiards are common systems to study chaotic dynamics and have been investigated thoroughly since the pioneering work of Sinai [12] and Bunimovich [13]. In two dimensions both regular and chaotic motions are possible. If in addition to the energy a conserved quantity exists, the dynamics is integrable. This is the case, e.g., for rectangles, circles, and ellipses. Stadium billiards, on the other hand, are known to be chaotic. In quantum mechanics the study of billiards with static walls became a central pillar in the theory of quantum

chaos [14–16]. Situations with moving boundaries have been investigated much less [17]. However, in recent years the interest in the classical dynamics of time-dependent billiards has grown. Integrable time-dependent billiards have been mainly discussed as toy models for Fermi acceleration [18–20]. The results are very interesting, but they all concern averages over a large number of particles. Quite generally, investigations of dynamical billiards that focus on the whole statistical distribution of energy are scarce [7,8,21].

The aim of this paper is to compare the classical and quantum work statistics of dynamical billiards with classically regular and chaotic behavior. The comparison can be used to analyze the quantum work statistic and to elucidate the consequences of classically chaotic behavior on the quantum case. Starting with one particle in a two-dimensional circular billiard, we consider two systems based on two types of expansion: first, a dynamical billiard system due to an expanding radius (System 1) and, second, a horizontal movement of the half circles in opposed directions building a Bunimovich stadium (System 2) [13]. This expansion step will be followed by a contraction step back to the initial circle.

We prepare the system in equilibrium with a heat bath at inverse temperature  $\beta = (k_B T)^{-1}$ . At time  $t = 0$  the bath and system are decoupled. During the expansion and the contraction the system is isolated from the environment. Because of the first law of thermodynamics the work is then given by the difference between initial energy  $E_0$  and final energy  $E$ . The work statistics

$$p(W) = \int_0^\infty dE \int_0^\infty dE_0 p_0(E_0) p(E|E_0) \delta[W - (E - E_0)] \quad (1)$$

involves the probability density  $p_0(E_0)$  to start in the initial energy  $E_0$  given by the Boltzmann distribution and the

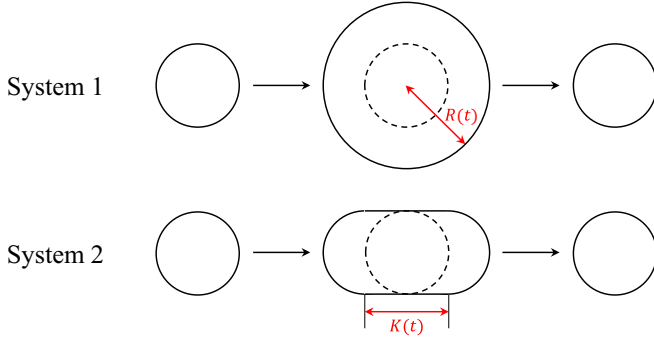


FIG. 1. The radially breathing circle (System 1) and the horizontally breathing stadium (System 2).

transition probability density  $p(E|E_0)$  to end with energy  $E$ .  $\delta(x)$  is the delta function.

The paper is organized as follows. In Sec. II we define System 1 and System 2 and describe them classically and quantum mechanically. Our results on the work statistics are given in Sec. III. Therein we start with the transition probability, Sec. III A, which leads to the work distribution, Sec. III B. In Secs. III C and III D we focus on the probability of no energy change ( $W = 0$ ) and no angular momentum change ( $\Delta L = 0$ ). Finally, Sec. IV contains our conclusion.

## II. TWO DYNAMICAL BILLIARD SYSTEMS

We start with a billiard system containing a two-dimensional circular edge with radius  $R_0$ . At time  $t = 0$  the system starts to expand with constant velocity  $u > 0$  up to time  $T/2$  (expansion phase) followed by a contraction phase with constant velocity  $-u$  for  $T/2 < t \leq T$  symmetric to the previous expansion. We consider two examples for the expansion and contraction phases:

- (i) With a radius varying linearly with time

$$R(t) = \begin{cases} R_0 + ut & t \leq T/2 \\ R_0 + u(T - t) & T/2 < t \leq T \end{cases} \quad (2)$$

in the following called System 1 and

- (ii) With a linear horizontal movement of the half circles in opposite directions forming a Bunimovich stadium billiard with an edge length

$$K(t) = \begin{cases} 2ut & t \leq T/2 \\ 2u(T - t) & T/2 < t \leq T \end{cases} \quad (3)$$

in the following called System 2.

Both systems are illustrated in Fig. 1. System 1 is a classically integrable system, whereas System 2 is chaotic. At  $t = T$  both billiards end in the initial circular billiard with radius  $R_0$ .

The quantity  $\frac{uT}{2R_0}$  is a dimensionless parameter in this system defining the strength of the process. We choose this parameter so that the characteristic length is double:

$$\frac{uT}{2R_0} = 1. \quad (4)$$

Note that all of the following calculation steps can be easily adapted to different parameters. However, for too small driving,  $\frac{uT}{2R_0} \ll 1$ , no nontrivial work distribution will occur. In

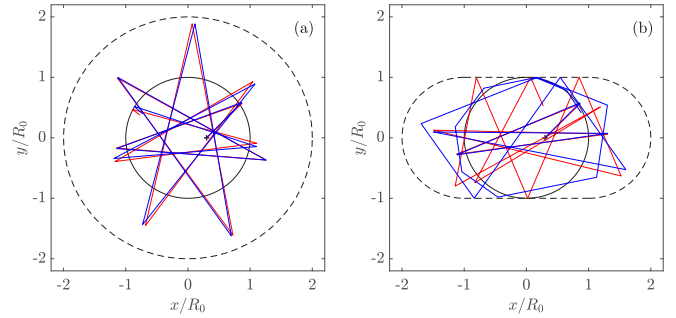


FIG. 2. Typical trajectories of classical particles at  $x_0 = 0.3R_0$ ,  $y_0 = 0$ ,  $v = 20u$  (bold plus sign) and a shooting angle of  $45^\circ$  (red) and  $46^\circ$  (blue) in (a) System 1 and (b) System 2.

the next subsections we first analyze the dynamics of classical particles in both systems and then the time evolution of wave functions.

### A. Classical description

For both systems we consider a classical particle starting at  $t = 0$  at position  $\mathbf{r}_0 = \begin{pmatrix} x_0 \\ y_0 \end{pmatrix}$  with velocity  $\mathbf{v}_0 = \begin{pmatrix} a_0 \\ b_0 \end{pmatrix}$ . The trajectory is a combination of rectilinear motions up to collisions with the walls. At each collision the particle velocity changes in modulus and in direction. For both systems the collision times, positions, and velocities are calculated analytically. In Appendix A explicit formulas are given for System 1, and a short discussion is given for System 2.

Two typical classical trajectories for both systems are shown in Fig. 2. The initial conditions are  $x_0 = 0.3R_0$ ,  $y_0 = 0$ , and  $v = 20u$ ; only the shooting angles differ:  $45^\circ$  and  $46^\circ$ . In System 1 both trajectories stay nearby as typical for regular systems, whereas in System 2 the trajectories differ strongly after a few collisions, which is characteristic for chaotic systems.

Using the same initial conditions as in Fig. 2 but with equidistant shooting angles in the full circle interval  $[0, 2\pi)$  the end points at  $t = T$  of all trajectories are plotted in Fig. 3. For System 1 adjacent shooting angles result in nearby end points, whereas in System 2 this behavior is not occurring even with a more accurate sampling. Also shown are the end energies  $E_f$  of these particles related by the initial energy  $E_0 = \frac{m}{2}v_0^2$ . We find that the energy spectrum of System 2 is broader than that of System 1.

### B. Quantum mechanical description

To describe the quantum dynamics we analyze the evolution of wave functions. As an initial wave function we start in an eigenstate of the static circular billiard. The time-independent Schrödinger equation is given by

$$E \psi = \left[ -\frac{\hbar^2}{2m} \left( \partial_\rho^2 + \frac{1}{\rho} \partial_\rho + \frac{\partial_\phi^2}{\rho^2} \right) + V(\rho) \right] \psi, \quad (5)$$

where  $V(\rho)$  vanishes inside the circle  $\rho \leq R_0$  and is infinite otherwise. The eigenstates are related to the Bessel functions

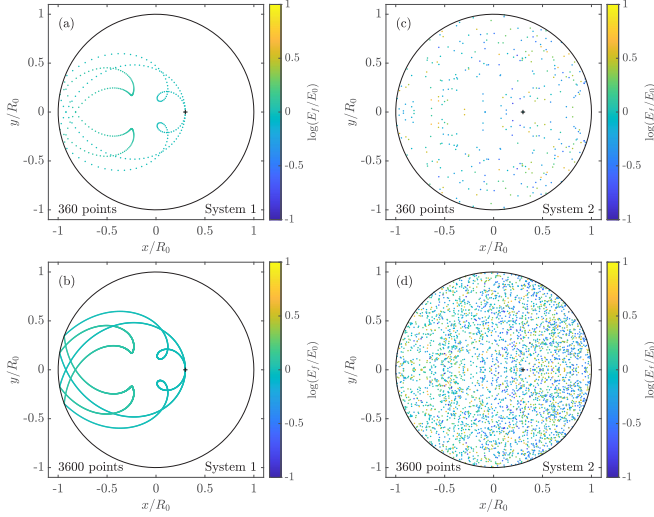


FIG. 3. Trajectory end points of classical particles with initial conditions  $x_0 = 0.3R_0$ ,  $y_0 = 0$  and  $v = 20u$  (bold plus sign) at different shooting angles between 0 and  $2\pi$  for System 1 (a, b) and (c, d). In (a) and (c) 360, and in (b) and (d) 3600 equidistant varying shooting angles are used. The color code shows the final energies.

of the first kind (see [21,22]):

$$\psi_{n,l}(\rho; R_0) = \frac{\mathcal{N}}{R_0} e^{i\phi} J_l\left(\frac{\rho}{R_0} j_{n,l}\right). \quad (6)$$

Here  $j_{n,l}$  denotes the  $n$ th zero of the  $l$ th Bessel function  $J_l$ . The main quantum number  $n = 1, 2, 3, \dots$  and the angular momentum quantum number  $l = 0, 1, 2, \dots$  specify the quantum state and are related to the angular momentum by

$$L = \hbar l \quad (7)$$

and to the energy by

$$E_{n,l} = \frac{\hbar^2}{2mR_0^2} j_{n,l}^2. \quad (8)$$

For System 1 we have to solve the time-dependent Schrödinger equation

$$i\hbar\partial_t\Psi = \left[ -\frac{\hbar^2}{2m} \left( \partial_\rho^2 + \frac{1}{\rho}\partial_\rho + \frac{\partial_\phi^2}{\rho^2} \right) + V(\rho, t) \right] \Psi, \quad (9)$$

where  $V(\rho, t)$  vanishes inside the circle  $\rho \leq R(t)$  and is infinite otherwise.  $R(t)$  is given by Eq. (2). This Schrödinger equation can be solved analytically [21], and the solution reads in the case of expansion,  $0 \leq t \leq \frac{T}{2}$ ,

$$\begin{aligned} \psi_{n,l}(\rho, t) = \exp\left[ -i \frac{\hbar^2 j_{n,l}^2 t - m^2 u \rho^2 R_0}{2\hbar m R_0 R(t)} \right] \\ \times \psi_{n,l}(\rho; R(t)), \end{aligned} \quad (10)$$

and in the case of contraction,  $\frac{T}{2} < t \leq T$ ,

$$\begin{aligned} \psi_{n,l}(\rho, t) = \exp\left[ -i \frac{\hbar^2 j_{n,l}^2 (t - \frac{T}{2}) + m^2 u \rho^2 R_{T/2}}{2\hbar m R_{T/2} R(t)} \right] \\ \times \psi_{n,l}(\rho; R(t)), \end{aligned} \quad (11)$$

where  $R_{T/2} = R(T/2)$ .

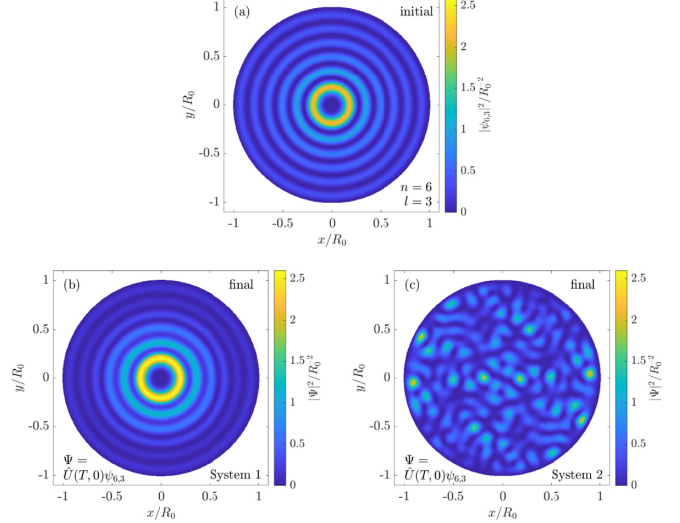


FIG. 4. Initial wave function for  $n = 6$  and  $l = 3$  (a) and its final state in System 1 (b) or in System 2 (c). The calculations were performed with parameters according to Eqs. (4) and (16).

The full quantum mechanical problem is solved by three expansions of the wave function: first, at  $t = 0$  in eigenstates of the time-dependent Schrödinger equation, Eq. (10); second, by expanding these wave functions at  $t = T/2$  in eigenstates of the contracting case at  $t = T/2$ , Eq. (11); and, third, by expanding these eigenstates at  $t = T$  in eigenstates of the stationary Schrödinger equation, Eq. (6).

Unlike System 1 the potential in System 2 is not radially symmetric. The time-dependent Schrödinger equation is given by

$$i\hbar\partial_t\Psi = \underbrace{\left[ -\frac{\hbar^2}{2m} (\partial_x^2 + \partial_y^2) + V(x, y, t) \right]}_{\hat{H}(t)} \Psi, \quad (12)$$

where  $V(x, y, t)$  vanishes inside the stadium and is infinite elsewhere.

We solve this Schrödinger equation with the spectral method [23]. Considering the formal solution

$$\Psi(t) = \hat{U}(t, 0)\Psi(0), \quad (13)$$

for short time steps  $\Delta t$  we use the time-evolution operator  $\hat{U}(t + \Delta t, t) \approx e^{-i\hat{H}(t)\Delta t/\hbar}$  to calculate iteratively the wave function in the next time step

$$\Psi(t + \Delta t) = e^{-i\hat{H}(t)\Delta t/\hbar}\Psi(t). \quad (14)$$

At each time step we split the time evolution operator into three parts,

$$e^{-i\hat{H}\Delta t/\hbar} \approx e^{i\frac{\hbar}{2m}\frac{\Delta t}{2}(\partial_x^2 + \partial_y^2)} e^{-i\hat{V}\Delta t/\hbar} e^{i\frac{\hbar}{2m}\frac{\Delta t}{2}(\partial_x^2 + \partial_y^2)}, \quad (15)$$

where the derivatives are calculated in Fourier space.

The different evolutions of a quantum mechanical wave function in an eigenstate of the initial circular billiard ( $n = 6$ ,  $l = 3$ ) are illustrated in Fig. 4 in which the squared moduli of the wave functions are plotted. Note that in the following all

quantum mechanical calculations are performed for

$$\frac{\hbar}{mR_0u} = 1 \Rightarrow j_{n,l} = \frac{v_0}{u}, \quad (16)$$

so the zeros of the Bessel functions are comparable to the classical velocity  $v_0$ . All of our calculations are also possible for any choice of  $\frac{\hbar}{mR_0u}$ . Note that smaller values of this parameter lead to higher quantum states at the beginning (assuming the starting energy remains the same) and we approach the classical limit.

Because of angular momentum conservation in System 1, the radial symmetry of the initial wave function is conserved. This is different from the final wave function after evolution in System 2. There the angular momentum is not conserved, and therefore the final wave function is not radially symmetric, it just shows the point symmetry of the system.

### III. RESULTS

#### A. Transition probabilities

Both dynamical billiard systems start and end in a circular billiard with radius  $R_0$ .

In classical mechanics the initial position  $\mathbf{r}_0$  and the velocity  $\mathbf{v}_0$  of a particle determine its final position  $\mathbf{r}_f$  and velocity  $\mathbf{v}_f$ . Nevertheless, the knowledge of the starting energy  $E_0$  and the angular momentum  $L_0$  is not enough to determine the final energy  $E$  and angular momentum  $L$ . For the statistics we express transitions via the joint conditional probability density  $p(E, L|E_0, L_0)$ , which gives the joint probability density of the final energy  $E$  and angular momentum  $L$  under the condition to start with the energy  $E_0$  and angular momentum  $L_0$ . This probability density is calculated by numerical simulation of  $10^5$  classical particles as discussed in Appendix A.

In the quantum case we represent the wave function at the end as a superposition of eigenstates of the circular billiard with radius  $R_0$ . Therefore, the probability for transitions from state  $(n_0, l_0)$  to  $(n, l)$  is given by

$$P(n, l|n_0, l_0) = |\langle \psi_{n,l} | \hat{U}(T, 0) | \psi_{n_0, l_0} \rangle|^2. \quad (17)$$

For a comparison of classical and quantum mechanical results we introduce the cumulative conditional probability of the final energy  $F(E|E_0)$ , which is classically defined by

$$F^{\text{cl}}(E|E_0) = \int_0^\infty dE' \int_{-\infty}^\infty dL \int_{-\infty}^\infty dL_0 \theta(E - E') \times p(E', L|E_0, L_0) p(L_0|E_0). \quad (18)$$

In the quantum case it is defined by

$$F^{\text{qm}}(E|E_{n_0, l_0}) = \sum_{n,l} \theta(E - E_{n,l}) P(n, l|n_0, l_0), \quad (19)$$

with the Heaviside function  $\theta(x) = \begin{cases} 0 & x < 0 \\ 1 & x \geq 0 \end{cases}$ .

For the initial conditions  $n_0 = 5$  and  $l_0 = 2$  ( $E_0 \approx 160mu^2$ ) the results are shown in Fig. 5. This is equivalent to a classical velocity  $v_0 \approx 18u$ . In the case of a fixed classical angular

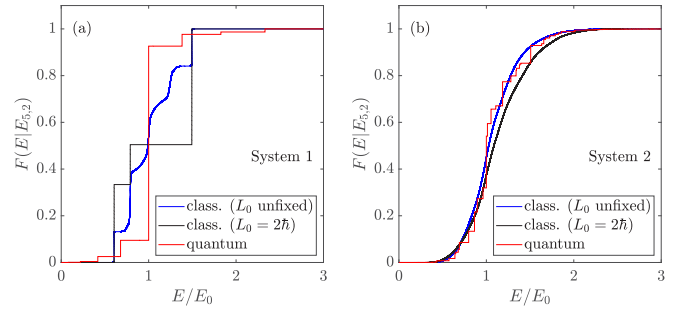


FIG. 5. Cumulative conditional probability for (a) System 1 and (b) System 2. Classical calculations were performed for  $10^5$  particles with an initial kinetic energy of  $E_{5,2}$  regardless of the angular momentum (blue) and with explicit consideration of  $L = \hbar l_0$  (solid black). In the quantum case (red) we start with a wave function in the eigenstate  $n_0 = 5$  and  $l_0 = 2$ . The calculations were performed with parameters according to Eqs. (4) and (16).

momentum  $L_0 = 2\hbar$  we find in System 1 a steplike function. For all collisions composing the jump the number  $n_e$  of energy losing collisions in the expanding phase is equal for all trajectories as well as the number  $n_k$  of energy gaining collisions in the contracting phase. In the first visible jump at  $E \approx 0.6E_0$  these numbers are  $n_e = 5$  and  $n_k = 3$ , in the second at  $E \approx 0.8E_0$  they are  $n_e = 5$  and  $n_k = 4$ , and in the last jump at  $E \approx 1.5E_0$  they are  $n_e = 4$  and  $n_k = 6$ . Other combinations are not observed. Because of the small angular momentum the particle velocity loss or gain per collision is almost always the same. Note that only in the special case  $L_0 = 0$  is the particle velocity change exactly  $2u$  per collision, which is the well-known result by particle collisions on moving walls [24]. With increasing values of  $L_0$  the energy loss or gain per collision fluctuates more. This leads to sigmoidal steps in the results at arbitrary (unfixed) angular momenta, which is a superposition of all possible angular momenta. Nevertheless, the dominant jump at lower  $L_0$  remains visible. The classical results in System 2 show a more continuous distribution for fixed angular momentum as well as for unfixed angular momenta, which is a consequence of the chaotic behavior. Indeed, each collision can be predicted analytically for given initial conditions, but small changes in these initial conditions will change dramatically the trajectory and the final conditions.

In System 1 the quantum mechanical result for the cumulative conditional probability shows a step function, which is the consequence of countably many transitions. Because of angular momentum conservation only transitions with  $l = l_0$  are allowed. In contrast to this the quantum mechanical calculations in System 2 show a quasicontinuous distribution, which is a consequence of the larger number of possible transitions. Independent of the considered system we conclude that classically forbidden energy transitions are unlikely in the quantum case.

#### B. Work distribution

Both systems are considered initially in thermal equilibrium with a bath at inverse temperature  $\beta$  and are decoupled from it at  $t = 0$ .

We first consider the classical case. Based on the first law of thermodynamics the work is related to the energy difference  $W = E - E_0$  and the cumulative work distribution  $F(W)$  is given by

$$F^{\text{cl}}(W) = \frac{1}{Z^{\text{cl}}} \int_0^\infty dE \int_0^\infty dE_0 e^{-\beta E_0} \times \theta(E_0 - E + W) p(E|E_0), \quad (20)$$

with the normalization  $Z^{\text{cl}} = \int_0^\infty dE_0 e^{-\beta E_0} = \beta^{-1}$ .

In calculation of the work in quantum systems we use the two projective measurements method which fulfills the Jarzynski equation  $\langle e^{-\beta W} \rangle = 1$  [5,25]: First, we measure the energy at the beginning  $t = 0$ . Hence we start in an eigenstate of the static circular billiard. After the second measurement at  $t = T$  we end in an eigenstate of the same static circular billiard with probability  $P(n, l|n_0, l_0)$ . The cumulative work distribution  $F(W)$  is given by

$$F^{\text{qm}}(W) = \frac{1}{Z^{\text{qm}}} \sum_{n,l,n_0,l_0} e^{-\beta E_{n_0,l_0}} \times \theta(E_{n_0,l_0} - E_{n,l} + W) P(n, l|n_0, l_0), \quad (21)$$

with the partition function  $Z^{\text{qm}} = \sum_{n_0,l_0} e^{-\beta E_{n_0,l_0}}$ .

For the following results we have verified the Jarzynski equation  $\langle e^{-\beta W} \rangle = 1$ , in the classical as well as in the quantum mechanical case. This is a consistency check for our numerical calculations.

The results for the cumulative work distribution for different temperatures represented by the dimensionless quantity

$$\tilde{\beta} = \frac{mu^2}{4} \beta \quad (22)$$

are shown in Fig. 6.  $\tilde{\beta}$  represents the quadratic ratio of the velocity  $u$  of the moving walls and the thermal velocity of the classical particles. In all figures the classical calculations were performed for  $10^5$  particles. For System 1 we recognize the sigmoidal steps from Fig. 5(a) and for System 2 the continuous distribution from Fig. 5(b). As expected in both systems, at higher temperatures (smaller values of  $\tilde{\beta}$ ) the width of the distribution gets broadened and the jump at  $W = 0$  decreases. These effects are also visible in the quantum mechanical results.

Contrary to what might be expected from the very different cumulative probability distributions in Fig. 5, the classical results for the work distribution for integrable System 1 look quantitatively similar to those for chaotic System 2. Since low-energy particles are primarily considered at low temperatures, there are only a few collisions. Therefore, a dominant step in  $F$  is seen at  $W = 0$ , and due to the geometry (starting and ending with the same circle in both systems) the steps in both systems are of about the same height. At higher temperatures, differences of a mainly quantitative nature around  $W = 0$  become visible. Moreover, in contrast to the chaotic System 2, the work distribution in System 1 exhibits a frequently changing curvature. This is a consequence of the sigmoidal

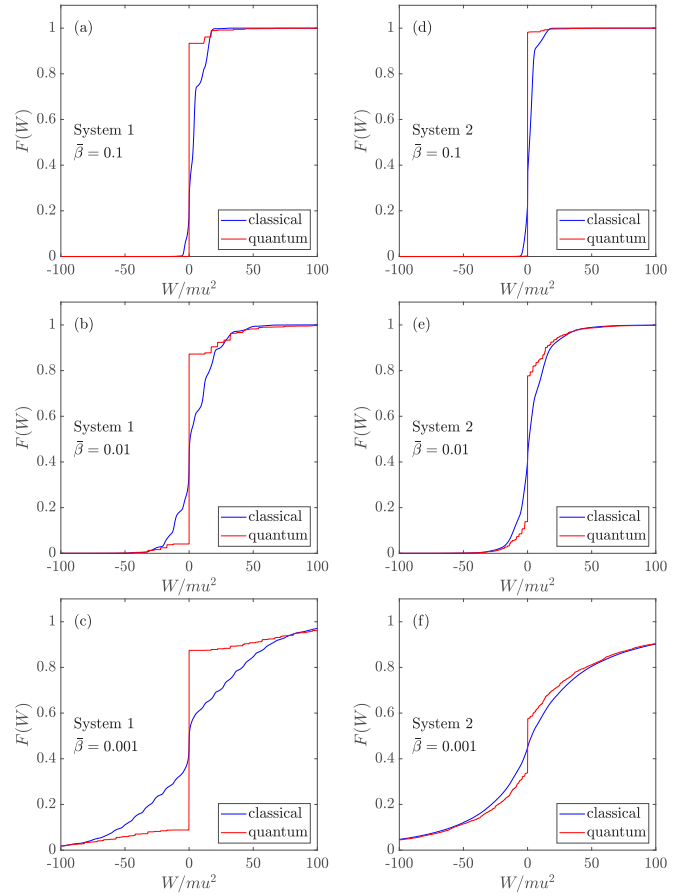


FIG. 6. Classical (blue) and quantum mechanical (red) cumulative work distribution at different temperatures  $1/\tilde{\beta}$  for (a–c) System 1 and (d–f) System 2. The calculations were performed with parameters according to Eqs. (4) and (16).

structure of  $F(E|E_0)$  shown in Fig. 5(a). These differences affect the quantum mechanical calculations.

Although the classical and quantum mechanical results for high temperatures converge in both systems, they are more pronounced in System 2. But note that this convergence is limited by the allowed transitions, which is explained in the following. Because of angular momentum conservation in System 1 the minimal positive value of work in the quantum case is limited by  $E_{2,0} - E_{1,0}$ ; cf. Eq. (8). This is different in System 2 in which transitions with angular momentum change are allowed too. These transitions might give smaller work values than  $E_{2,0} - E_{1,0}$ . For example, when taking into account the 1000 lowest states we find 2823 possible transitions inside the work interval  $(0, E_{2,0} - E_{1,0})$  in System 2, whereas we find no transitions in System 1. So in System 1 many work values are forbidden, which is not the case in System 2. As a consequence we see a marked difference between the steps at  $W = 0$  in Figs. 6(c) and 6(f).

Note that using the thermal velocity instead of  $u$  in Eq. (16), a parameter for the quantumness of the system can be introduced,  $\frac{\hbar\sqrt{\beta}}{R_0\sqrt{m}}$ . All of our calculation steps can be easily adapted to different values for the quantumness, and an extended analysis is possible.

### C. Probability of no energy change

In both systems there is a nonzero probability that the processes occur without performing mechanical work at all. This happens in the quantum as well as in the classical one; see Fig. 6.

In the classical case of System 1 any collisions yield an energy change. Only selected combinations of collisions lead to exactly the same initial energies. Such combinations are improbable and will not be considered further. The probability of zero collisions is derived in Appendix B as

$$P_1^{\text{cl}}(W = 0) = 1 - e^{-\bar{\beta}}[I_0(\bar{\beta}) + I_1(\bar{\beta})], \quad (23)$$

where  $I_0$  and  $I_1$  are modified Bessel's functions of the first kind, and  $\bar{\beta}$  is defined in Eq. (22).

In contrast to this in System 2 there exists a nonzero probability to perform collisions with the horizontal walls of the stadium only which conserve the energy. So the condition of zero collisions is sufficient but not necessary for  $W = 0$ . Hence, we expect  $P_1^{\text{cl}}(W = 0) \leq P_2^{\text{cl}}(W = 0)$  as a lower limit. Also an upper limit can be derived:

$$P_2^{\text{cl}}(W = 0) \leq P_1^{\text{cl}}(W = 0) + \sum_{k=1}^{\infty} \frac{2\bar{\beta}}{\pi} \int_{2k-2}^{2k} dx x e^{-\frac{\bar{\beta}}{2}x^2} \times \int_{2k-1}^{1+x} dy f(x, y) \arcsin \sqrt{\frac{16k^2 - (y^2 - 1 - 4k^2)^2}{16k^2 y^2}}, \quad (24)$$

$$f(x, y) = y - \frac{2y}{\pi} \arctan \left[ \frac{-1 + y^2 + x^2}{\sqrt{-y^4 - (1-x)^2 + 2y^2(1+x^2)}} \right]. \quad (25)$$

For details see Appendix B.

Because the eigenvalues in the quantum case are not degenerated, a vanishing work is a consequence of self-transitions. So the probability  $P(W = 0)$  is related to the trace of the transition probabilities

$$P^{\text{qm}}(W = 0) = \frac{1}{Z^{\text{qm}}} \sum_{n_0, l_0} e^{-\beta E_{n_0, l_0}} P(n_0, l_0 | n_0, l_0). \quad (26)$$

As a consequence angular momentum conservation is a necessary condition for  $W = 0$ .

For System 1 the analytical formula Eq. (23) matches accurately the numerical simulations of  $10^5$  classical particles per point; see Fig. 7(a). We find similarly good results for Eqs. (23) and (24), which limit the probability  $P(W = 0)$  for classical particles in System 2; see Fig. 7(b). As already mentioned in Sec. III B the probability  $P(W = 0)$  decreases with higher temperatures (small  $\beta$ ) in the classical as well as in the quantum case. But different from the classical case where  $P_2^{\text{cl}}(W = 0) \geq P_1^{\text{cl}}(W = 0)$ , at higher temperatures we find  $P_2^{\text{qm}}(W = 0) < P_1^{\text{qm}}(W = 0)$ ; cf. Fig. 6. This is related to the forbidden transitions in System 1 as discussed at the end

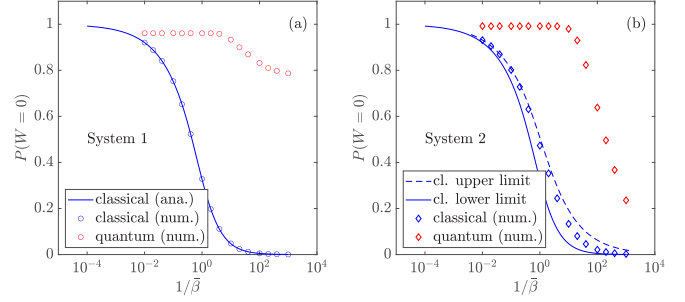


FIG. 7. Classical (blue) and quantum mechanical (red) probability of no energy change depending on temperature  $1/\beta$  for (a) System 1 and (b) System 2. The blue solid lines are given by Eq. (23), and the dashed line is given by Eq. (24). The calculations were performed with parameters according to Eqs. (4) and (16).

of Sec. III B. In addition it seems that in System 1 the value of  $P_1^{\text{qm}}(W = 0)$  converges at high temperatures to a nonzero plateau.

### D. Probability of no angular momentum change

The results for the work statistics presented in Sec. III B and III C arise from by marginalization of the transition probabilities introduced in Sec. III A with respect to the angular momenta. In this section we consider these transition probabilities again. But now we marginalize with respect to the energies and calculate the probability of no angular-momentum change. This leads on the one hand to fundamental differences between the classical and quantum case and on the other hand to a connection between both systems.

System 1 is radially symmetric at all times and the Hamiltonian is not explicitly angular-dependent, so the angular momentum is a conserved quantity and

$$P_1(\Delta L = 0) = 1 \quad (27)$$

is trivial in both classical and quantum mechanics.

This is different in System 2, which is only radially symmetric at the beginning and at the end. Except special initial conditions, in the classical case all collisions (also those that the particle performs with the resting horizontal edges and conserve the energy) change the angular momentum. Except for the occasional one further collisions cannot compensate this change exactly. It follows

$$P_2^{\text{cl}}(\Delta L = 0) = 1 - e^{-\bar{\beta}}[I_0(\bar{\beta}) + I_1(\bar{\beta})], \quad (28)$$

with  $\bar{\beta}$  defined in Eq. (22). The r.h.s. is identical with that in Eq. (23) since it represents the probability of no collisions. For details see Appendix B. So  $P_2^{\text{cl}}(\Delta L = 0) \leq P_2^{\text{cl}}(W = 0)$  is trivial; see Eq. (24).

In contrast to this is the quantum mechanical case. Indeed, quantum mechanical transitions which change the parity of angular quantum numbers are forbidden, but other transitions  $\Delta L = 0, 2, 4, \dots$  are allowed. Note that all transitions (also those changing the main quantum number) which conserve the angular momentum quantum number contribute to

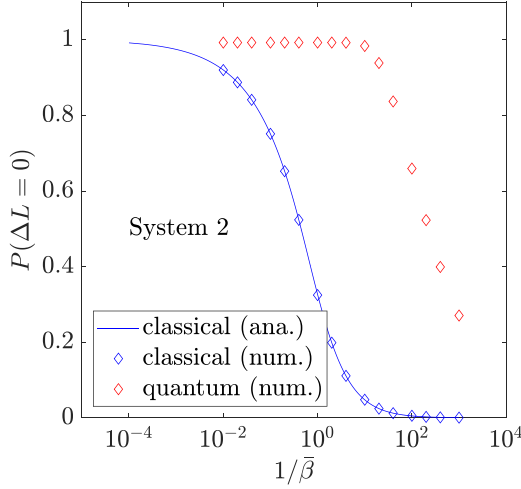


FIG. 8. Classical (blue) and quantum mechanical (red) probability of no angular momentum change depending on temperature  $1/\bar{\beta}$  for System 2. The blue solid line is given by Eq. (28). The calculations were performed with parameters according to Eqs. (4) and (16).

$P(\Delta L = 0)$ ,

$$P_2^{\text{qm}}(\Delta L = 0) = \frac{1}{Z^{\text{qm}}} \sum_{n, n_0, l_0} e^{-\beta E_{n_0, l_0}} P(n, l_0 | n_0, l_0), \quad (29)$$

and especially it follows that  $P_2^{\text{qm}}(\Delta L = 0) \geq P_2^{\text{qm}}(W = 0)$ ; see Eq. (26).

These effects are illustrated in Fig. 8. Similarly to the previous section formula, Eq. (28) matches accurately the numerical simulations of  $10^5$  classical particles per point. Comparing with Fig. 7(b) in which the numerical results lie above the full line, we see our numerical results confirm the expectation  $P_2^{\text{cl}}(\Delta L = 0) \leq P_2^{\text{cl}}(W = 0)$ . Of course, the quantum mechanical numerical results confirm  $P_2^{\text{qm}}(\Delta L = 0) \geq P_2^{\text{qm}}(W = 0)$ . This is trivial since Eqs. (26) and (29) are used for these calculations, respectively. As in Fig. 7(b) the quantum values for  $P_2^{\text{qm}}(\Delta L = 0)$  decrease for higher temperatures.

#### IV. CONCLUSION

The aim of this paper is to contribute to the field of quantum work statistics. We have chosen two two-dimensional billiard systems, one of which is a classically integrable breathing circle (System 1) and the other one forms a classical-chaotic stadium (System 2).

Both systems are characterized by three dimensionless parameters. The first one  $\frac{uT}{2R_0}$  gives the process strength. If it is reduced, the variation of the systems gets smaller compared to the whole system. We expect that the variation of the work decreases and the distribution becomes sharper. The second parameter  $\bar{\beta}$  connects the velocity  $u$  of the moving walls with the thermal velocity of the heat bath. In particular the dependence on this parameter has been analyzed in more detail. The third parameter  $\frac{\hbar\sqrt{\bar{\beta}}}{k_0\sqrt{m}}$  gives the quantumness of the initial state. If this one decreases, the systems approach the classical limit.

Classical calculations of trajectories have been performed iteratively. For the quantum mechanical calculations we have solved the time-dependent Schrödinger equation. Whereas there is an analytical solution for System 1, the evolution of wave functions in System 2 has been solved by the spectral method. Using these ingredients the classical conditional probability density  $p(E, L|E_0, L_0)$  as well as the quantum mechanical transition probability  $P(n, l|n_0, l_0)$  follow, which build the basis for the statistical analysis.

So it has been possible to calculate the work distribution for a particle in such systems. The results in the quantum case especially are of particular interest since a suitable definition of mechanical work in small quantum systems is already controversial. We find that for higher temperatures the classical and quantum mechanical work distributions converge to each other. Nevertheless, on the one hand this convergence in System 1 is limited. There are temperature-independent barriers because of angular momentum conservation; e.g., values of work between 0 and  $E_{2,0} - E_{1,0}$  are forbidden. For System 2 there cannot exist such barriers. On the other hand, a rapidly increasing number of eigenstates has to be calculated. At this point semiclassical methods become of relevance which may build a connection between very fast classical simulations and very cumbersome quantum mechanical calculations. The semiclassical analysis of these systems is part of further research.

Furthermore, we present the results for the probability of no energy or no angular momentum change. Using connections to an exactly solvable system, analytical formulas are given for these classical probabilities in both systems. These formulas may be applied to other classical billiard systems. For System 2 it is trivial to see that in the classical case all collisions (except for the occasional one) yield an angular momentum change. Collisions with the horizontal walls did not change the energy. So the probability of no angular momentum change is lower than the probability of no energy change,  $P_2^{\text{cl}}(\Delta L = 0) \leq P_2^{\text{cl}}(W = 0)$ . This is in contrast to the quantum case,  $P_2^{\text{qm}}(\Delta L = 0) \geq P_2^{\text{qm}}(W = 0)$ . Also here semiclassical methods may clarify this fundamental difference. For example, in the classical case  $\Delta L = 0$  is a very specific situation. All situations  $\Delta L \approx 0$  will be included in the quantized angular momentum change  $\Delta L = 0$  by semiclassical methods. This could be the reason for the fundamental change of the inequality.

In this paper we assumed a linear  $t$  dependence of the varying radius and edge length. But other  $t$  dependencies can be treated in the same way. For special time dependencies the time-dependent Schrödinger equation for System 1 can be solved analytically; see [21]. But the numerical calculation for System 2 can be used for System 1 too.

#### ACKNOWLEDGMENTS

We would like to thank Andreas Engel, Axel Prüser, and the members of the DFG Research Unit FOR2692 for fruitful discussions. This work has been funded by the Deutsche Forschungsgemeinschaft (DFG, German Research Foundation), Grant No. 397082825.

**APPENDIX A: CLASSICAL DESCRIPTIONS  
OF SYSTEM 1 AND 2**

**a. Radial breathing circle (System 1)**

If the particle velocity is larger than the expansion velocity of the circle  $|\mathbf{v}| > u$ , the first collision occurs at

$$t_1 = \frac{uR_0 - \mathbf{r}_0\mathbf{v}_0}{v_0^2 - u^2} + \Delta(u, R_0, \mathbf{r}_0, \mathbf{v}_0), \quad (\text{A1})$$

$$\Delta(u, R_0, \mathbf{r}_0, \mathbf{v}_0) = \sqrt{\left(\frac{uR_0 - \mathbf{r}_0\mathbf{v}_0}{v_0^2 - u^2}\right)^2 + \frac{R_0^2 - r_0^2}{v_0^2 - u^2}}, \quad (\text{A2})$$

at position

$$\mathbf{R}_1 = \mathbf{r}_0 + \mathbf{v}_0 t_1, \quad (\text{A3})$$

if  $t_1 < T/2$ . If  $t_1 \geq T/2$  or  $|\mathbf{v}| \leq u$ , there is no collision in the expanding phase, and the particle position and velocity at  $t = T/2$  are

$$\bar{\mathbf{r}}_0 = \mathbf{r}_0 + \mathbf{v}_0 \frac{T}{2}, \quad (\text{A4})$$

$$\bar{\mathbf{v}}_0 = \mathbf{v}_0. \quad (\text{A5})$$

At each collision during the expanding phase the radial part of the particle velocity is decreased by  $2u$ , whereas the angular part stays constant; in the  $j$ th collision the velocity  $\mathbf{v}_{j-1}$  changes by

$$\mathbf{v}_j = \mathbf{v}_{j-1} - 2 \frac{uR_j - \mathbf{R}_j\mathbf{v}_{j-1}}{R_j^2} \mathbf{R}_j. \quad (\text{A6})$$

If  $v_j^2 > u^2$  the next collision time is determined by

$$t_{j+1} = 2 \frac{uR_j - \mathbf{R}_j\mathbf{v}_j}{v_j^2 - u^2} \quad j \geq 1. \quad (\text{A7})$$

The collision position is

$$\mathbf{R}_{j+1} = \mathbf{R}_j + \mathbf{v}_j t_{j+1}. \quad (\text{A8})$$

The smallest  $j = J$  for which either  $v_j^2 \leq u^2$  or  $\sum_{n=1}^{J+1} t_n > T/2$  is the number of collisions in the expanding phase; so for the particle position and velocity at  $t = T/2$  follow

$$\bar{\mathbf{r}}_0 = \mathbf{R}_J + \mathbf{v}_J \left( \frac{T}{2} - \sum_{n=1}^J t_n \right), \quad (\text{A9})$$

$$\bar{\mathbf{v}}_0 = \mathbf{v}_J. \quad (\text{A10})$$

In the contracting phase ( $u \rightarrow \bar{u} = -u$ ,  $\bar{R}_0 = R_0 + u \frac{T}{2}$ ) the first collision occurs at

$$\bar{t}_1 = \begin{cases} \frac{\bar{u}\bar{R}_0 - \bar{\mathbf{r}}_0\bar{\mathbf{v}}_0}{\bar{v}_0^2 - \bar{u}^2} + \Delta(\bar{u}, \bar{R}_0, \bar{\mathbf{r}}_0, \bar{\mathbf{v}}_0) & \bar{v}_0^2 > \bar{u}^2 \\ \frac{\bar{u}\bar{R}_0 - \bar{\mathbf{r}}_0\bar{\mathbf{v}}_0}{\bar{v}_0^2 - \bar{u}^2} - \Delta(\bar{u}, \bar{R}_0, \bar{\mathbf{r}}_0, \bar{\mathbf{v}}_0) & \bar{v}_0^2 < \bar{u}^2 \\ \frac{\bar{R}_0^2 - \bar{r}_0^2}{2(\bar{\mathbf{r}}_0\bar{\mathbf{v}}_0 - \bar{R}_0\bar{u})} & \bar{v}_0^2 = \bar{u}^2, \end{cases} \quad (\text{A11})$$

on position

$$\bar{\mathbf{R}}_1 = \bar{\mathbf{r}}_0 + \bar{\mathbf{v}}_0 \bar{t}_1, \quad (\text{A12})$$

if  $\bar{t}_1 \leq \frac{T}{2}$ . In the case  $\bar{t}_1 > \frac{T}{2}$  there is no collision in the contracting phase, and the final particle position and velocity

are

$$\mathbf{r}_f = \bar{\mathbf{r}}_0 + \bar{\mathbf{v}}_0 \frac{T}{2}, \quad (\text{A13})$$

$$\mathbf{v}_f = \bar{\mathbf{v}}_0. \quad (\text{A14})$$

At each collision during the contraction phase the radial part of the particle velocity is increased by  $2u$ , whereas the angular part stays constant; in the  $k$ th collision the velocity  $\bar{\mathbf{v}}_{k-1}$  changes by

$$\bar{\mathbf{v}}_k = \bar{\mathbf{v}}_{k-1} - 2 \frac{\bar{u}\bar{R}_k - \bar{\mathbf{R}}_k\bar{\mathbf{v}}_{k-1}}{\bar{R}_k^2} \bar{\mathbf{R}}_k. \quad (\text{A15})$$

The next collision time is determined by

$$\bar{t}_{k+1} = 2 \frac{\bar{u}\bar{R}_k - \bar{\mathbf{R}}_k\bar{\mathbf{v}}_k}{\bar{v}_k^2 - \bar{u}^2} \quad k \geq 1, \quad (\text{A16})$$

at position

$$\bar{\mathbf{R}}_{k+1} = \bar{\mathbf{R}}_k + \bar{\mathbf{v}}_k \bar{t}_{k+1}. \quad (\text{A17})$$

The lowest  $k = K$  for which  $\sum_{n=1}^{K+1} \bar{t}_n > T/2$  is the number of collisions in the contracting phase; so the final particle position and velocity are

$$\mathbf{r}_f = \bar{\mathbf{R}}_K + \bar{\mathbf{v}}_K \left( \frac{T}{2} - \sum_{n=1}^K \bar{t}_n \right), \quad (\text{A18})$$

$$\mathbf{v}_f = \bar{\mathbf{v}}_K. \quad (\text{A19})$$

**b. Horizontal breathing stadium (System 2)**

In the following we give the explicit formulas for the first collision time and position in the cases  $x_0 \geq 0$  and  $y_0 \geq 0$  assuming the first collision takes place in the expanding phase. For all other cases as well as for further collisions and collisions in the contraction phase the explicit formulas can be derived in a similar way.

The initial velocity is  $\mathbf{v}_0 = \begin{pmatrix} a_0 \\ b_0 \end{pmatrix}$ . If  $b_0 = 0$  and  $|a_0| < u$ , no collision will happen in the expansion phase. For  $b_0 = 0$  and  $a_0 < -|u|$  the first collision occurs at the left half circle, and for  $a_0 > |u|$  (independent of  $b_0$ ) the first collision occurs at the right half circle. In all other cases the location of the first collision (left or right half circle or static top or bottom line) depends on three characteristic times:

1. The escape time from the right half circle  $t^{(I)} = \frac{x_0}{|u| - a_0}$ , only relevant if  $a_0 < |u|$

2. The collision time at the top ( $b_0 > 0$ ) or bottom ( $b_0 < 0$ ) line  $t^{(II)} = \frac{\text{sgn}(b_0)R_0 - y_0}{b_0}$  and

3. The entry time to the left half circle  $t^{(III)} = \frac{-x_0}{|u| + a_0} > t^{(I)}$ , relevant only if  $a_0 < -|u|$ .

If  $t^{(II)} < t^{(I)}$  or  $a_0 > u$ , the first collision will occur at the right half circle at time  $t_1$  at position  $\mathbf{R}_1$  and the velocity changes to  $\mathbf{v}_1$ :

$$t_1 = \frac{-(a_0 - u)x_0 - b_0 y_0}{(a_0 - u)^2 + b_0^2} + \sqrt{\left[ \frac{-(a_0 - u)x_0 - b_0 y_0}{(a_0 - u)^2 + b_0^2} \right]^2 + \frac{R^2 - x_0^2 - y_0^2}{(a_0 - u)^2 + b_0^2}}, \quad (\text{A20})$$



$$\mathbf{R}_1 = \begin{pmatrix} X_1 \\ Y_1 \end{pmatrix} = \mathbf{r}_0 + \mathbf{v}_0 t_1, \quad (\text{A21})$$

$$\mathbf{v}_1 = \frac{1}{R_0^2} \begin{pmatrix} uR_0^2 + (a_0 - u)[Y_1^2 - (X_1 - ut_1)^2] - 2b_0(X_1 - ut_1)Y_1 \\ b_0[(X_1 - ut_1)^2 - Y_1^2] - 2(a_0 - u)(X_1 - ut_1)Y_1 \end{pmatrix}. \quad (\text{A22})$$

Otherwise if  $t^{(\text{I})} < t^{(\text{II})} < t^{(\text{III})}$ , the first collision will occur at the static top or bottom line at time

$$t_1 = t^{(\text{II})} \quad (\text{A23})$$

at position

$$\mathbf{R}_1 = \mathbf{r}_0 + \mathbf{v}_0 t_1, \quad (\text{A24})$$

and the velocity changes to

$$\mathbf{v}_1 = \begin{pmatrix} a_0 \\ -b_0 \end{pmatrix}. \quad (\text{A25})$$

Else the first collision will occur at the left half circle at time  $t_1$  at position  $\mathbf{R}_1$  and the velocity changes to  $\mathbf{v}_1$ :

$$t_1 = t^{(\text{III})} - \frac{(y_0 + b_0 t^{(\text{III})})b_0}{(a_0 + u)^2 + b_0^2} + \sqrt{\left[ \frac{(y_0 + b_0 t^{(\text{III})})b_0}{(a_0 + u)^2 + b_0^2} \right]^2 + \frac{R^2 - (y_0 + b_0 t^{(\text{III})})^2}{(a_0 + u)^2 + b_0^2}}, \quad (\text{A26})$$

$$\mathbf{R}_1 = \begin{pmatrix} X_1 \\ Y_1 \end{pmatrix} = \mathbf{r}_0 + \mathbf{v}_0 t_1, \quad (\text{A27})$$

$$\mathbf{v}_1 = \frac{1}{R_0^2} \begin{pmatrix} -uR_0^2 + (a_0 + u)[Y_1^2 - (X_1 + ut_1)^2] - 2b_0(X_1 + ut_1)Y_1 \\ b_0[(X_1 + ut_1)^2 - Y_1^2] - 2(a_0 + u)(X_1 + ut_1)Y_1 \end{pmatrix}. \quad (\text{A28})$$

After each collision the new position and the new velocity determine at which wall (left or right half circle or top or bottom line) the next collision will happen. The velocity change depends on that wall; see Eqs. (A22), (A25), and (A28), respectively. A simple closed form of  $t_1$ ,  $\mathbf{R}_1$ , and  $\mathbf{v}_1$  does not exist.

Nevertheless, similar considerations as for the first collision may be done for further collisions up to  $t = T/2$  as well as for collisions in the contracting phase.

## APPENDIX B: CLASSICAL PROBABILITY OF NO ENERGY CHANGE AND NO ANGULAR MOMENTUM CHANGE

We consider a static circular billiard with radius  $R_0$  in thermal equilibrium with a heat bath at inverse temperature  $\beta$ . At  $t = 0$  system and bath are decoupled, and we remove the walls. This system is referred to as System 0. The detailed relations with Systems 1 and 2 are explained below.

In System 0, all particles perform a rectilinear motion. The distance to the center of the initial circle is given at time  $T$  by

$$r_T(r_0, \varphi; vT) = \sqrt{(r_0 + vT \cos \varphi)^2 + (vT)^2 \sin^2 \varphi} \quad (\text{B1})$$

depending on the initial distance  $r_0$  (linearly distributed), the launching angle  $\varphi$  (uniformly distributed), and the length of path  $vT$ . Hence,  $r_T$  is a stochastic variable with distribution

$$p^{(0)}(r_T; vT) = \langle \delta[r_T(r_0, \varphi; vT) - r_T] \rangle_{r_0, \varphi}, \quad (\text{B2})$$

$$\langle (\cdot) \rangle_{r_0, \varphi} = \int_0^{R_0} dr_0 \int_0^{2\pi} d\varphi (\cdot) p(r_0) p(\varphi). \quad (\text{B3})$$

This double integral can be performed analytically:

$$p^{(0)}(r_T; vT) = \begin{cases} \frac{2r_T}{R_0^2} & 0 \leq r_T \leq \max\{0; R_0 - vT\} \\ \frac{r_T}{R_0^2} - \frac{2r_T}{\pi R_0^2} \arctan \left\{ \frac{-R_0^2 + r_T^2 + (vT)^2}{\sqrt{-r_T^4 - (R_0 - vT)^2 R_0^2 + 2r_T^2 [R_0^2 + (vT)^2]}} \right\} & \max\{0; R_0 - vT\} \leq r_T < R_0 + vT \\ 0 & \text{otherwise.} \end{cases} \quad (\text{B4})$$

In a canonical ensemble at the beginning the velocity of a particle  $v(E)$  is Maxwell distributed. The probability that this particle is at  $t = T$  and still be found inside the initial circle (with radius  $R_0$ ) is given by

$$P_0(r_T \leq R_0) = \int_0^\infty dE \beta e^{-\beta E} \int_0^{R_0} dr_T p^{(0)}(r_T; v(E)T) = 1 - e^{-\bar{\beta}} [I_0(\bar{\beta}) + I_1(\bar{\beta})], \quad (\text{B5})$$

$$\bar{\beta} = \frac{mR_0^2}{T^2} \beta,$$

where  $I_0$  and  $I_1$  are modified Bessel's functions of the first kind.

The probability  $P_0(r_T \leq R_0)$  is equal to the probability in System 1 and 2 that no collisions were performed, so

$$P_0(r_T \leq R_0) = P_1^{\text{cl}}(W = 0), \quad (\text{B6})$$

$$P_0(r_T \leq R_0) = P_2^{\text{cl}}(\Delta L = 0) \leq P_2^{\text{cl}}(W = 0). \quad (\text{B7})$$

Especially for System 1 any collision or combinations of collisions change the energy of the classical velocity except for the occasional one. Only fine-tuned combinations of starting positions and launching angles are able to compensate energy loss and energy gain exactly.

To find an upper limit for  $P_2^{\text{cl}}(W = 0)$  the treatment of the reflections in System 2 with the horizontal resting walls is of particular interest. For this, we consider the probability density of System 0 again, Eq. (B4). Imagine a chain of equal-sized adjacent circles along the  $y$  axis and the initial circle is one of them in the center. With a canonical velocity distribution the probability of presence in the  $k$ th circle above or below the initial circle can be simplified to

$$P_{00} = P_0(r_T \leq R_0), \quad (\text{B8})$$

$$P_{0k} = \bar{\beta} \int_{2k-2}^{2k} dx x e^{-\frac{\beta}{2}x^2} \times \int_{(2k-1)R_0}^{(1+x)R_0} dr_T p^{(0)}(r_T; xR_0) \Pi_k(r_T), \quad (\text{B9})$$

where  $\Pi_k(r_T)$  is the weight that states which particle fraction is inside the  $k$ th circle above or below:

$$\Pi_k(r_T) = \frac{2}{\pi} \arcsin \left[ \frac{\sqrt{16k^2 R_0^4 - (r_T^2 - R_0^2 - 4k^2 R_0^2)^2}}{4kr_T R_0} \right].$$

A reflection in System 2 with the horizontal resting walls can be projected as a mirrored trajectory which entered a

stadium above or below. Therefore, we consider a particle in System 2 which collides only on the horizontal walls. In System 0 the same particle has to be located in the initial circle or in one of the imagined circles (above or below). Note that the inversion does not apply. So its probability of presence in one of these circles is an upper limit for  $P_2^{\text{cl}}(W = 0)$  in System 2 and

$$P_2^{\text{cl}}(W = 0) \leq \sum_{k=0}^{\infty} P_{0k}. \quad (\text{B10})$$

Substituting  $y = r_T/R_0$ , Eqs. (B8)–(B10) combine to the upper limit Eq. (24).

- 
- [1] C. Jarzynski, *Annu. Rev. Condens. Matter Phys.* **2**, 329 (2011).  
 [2] U. Seifert, *Rep. Prog. Phys.* **75**, 126001 (2012).  
 [3] S. Yukawa, *J. Phys. Soc. Jpn.* **69**, 2367 (2000).  
 [4] P. Talkner and P. Hänggi, *Phys. Rev. E* **93**, 022131 (2016).  
 [5] A. Engel and R. Nolte, *Europhys. Lett.* **79**, 10003 (2007).  
 [6] F. Binder, L. A. Correa, C. Gogolin, J. Anders, and G. Adesso, *Thermodynamics in the Quantum Regime: Fundamental Aspects and New Directions*, Fundamental Theories of Physics Vol. 195 (Springer International Publishing, Cham, Switzerland, 2018).  
 [7] I. García-Mata, A. J. Roncaglia, and D. A. Wisniacki, *Phys. Rev. E* **95**, 050102(R) (2017).  
 [8] I. García-Mata, A. J. Roncaglia, and D. A. Wisniacki, *Europhys. Lett.* **120**, 30002 (2017).  
 [9] C. Jarzynski, H. T. Quan, and S. Rahav, *Phys. Rev. X* **5**, 031038 (2015).  
 [10] M. Engbers, M. Heerwagen, S. Rosmej, and A. Engel, *Z. Naturforsch.* **75**, 433 (2020).  
 [11] M. Heerwagen and A. Engel, *Phys. Rev. E* **102**, 022121 (2020).  
 [12] Y. G. Sinai, *Russ. Math. Surv.* **25**, 137 (1970).  
 [13] L. A. Bunimovich, *Commun. Math. Phys.* **65**, 295 (1979).  
 [14] B. Eckhardt, *Phys. Rep.* **163**, 205 (1988).  
 [15] M. C. Gutzwiller, *Chaos in Classical and Quantum Mechanics* (Springer, New York, 1990).  
 [16] H.-J. Stöckmann, *Quantum Chaos: An Introduction* (Cambridge University Press, Cambridge, 2000).  
 [17] J. Deng, A. M. Tan, P. Hänggi, and J. Gong, *Phys. Rev. E* **95**, 012106 (2017).  
 [18] A. Loskutov, A. B. Ryabov, and L. G. Akinshin, *J. Phys. A: Math. Gen.* **33**, 7973 (2000).  
 [19] F. Lenz, C. Petri, F. N. R. Koch, and P. Schmelcher, *A Fresh View on Fermi Acceleration in Driven Two-Dimensional Billiards* (Springer Netherlands, Dordrecht, 2009).  
 [20] K. Nakamura, S. K. Avazbaev, Z. A. Sobirov, D. U. Matrasulov, and T. Monnai, *Phys. Rev. E* **83**, 041133 (2011).  
 [21] D. Babajanov, D. Matrasulov, Z. Sobirov, S. Avazbaev, and O. V. Karpova, *Nanosyst.: Phys. Chem. Math.* **6**, 224 (2015).  
 [22] M. Abramowitz and I. A. Stegun, *Handbook of Mathematical Functions* (National Bureau of Standards, Washington, DC, 1972).  
 [23] M. D. Feit, J. A. Fleck, and A. Steiger, *J. Comput. Phys.* **47**, 412 (1982).  
 [24] L. D. Landau and E. M. Lifshitz, *Course of Theoretical Physics I: Mechanics* (Butterworth-Heinemann, Oxford, 2011), Sec. 17.  
 [25] C. Jarzynski, *Phys. Rev. Lett.* **78**, 2690 (1997).